Downloaded from rsta.royalsocietypublishing.org on October 7, 2013

PHILOSOPHICAL TRANSACTIONS OF THE ROYAL SOCIETY A
MATHEMATICAL, PHYSICAL & ENGINEERING SCIENCES

Future trends in aberration-corrected electron microscopy

Harald H. Rose

Phil. Trans. R. Soc. A 2009 **367**, doi: 10.1098/rsta.2009.0062, published 17 August 2009

Supplementary data "Audio Supplement"
http://rsta.royalsocietypublishing.org/content/suppl/2009/08/11/367.1903.3809.DC1.html

References **This article cites 10 articles**
http://rsta.royalsocietypublishing.org/content/367/1903/3809.full.html#ref-list-1

Subject collections Articles on similar topics can be found in the following collections

electron microscopy (18 articles)

Email alerting service Receive free email alerts when new articles cite this article - sign up in the box at the top right-hand corner of the article or click **here**

To subscribe to *Phil. Trans. R. Soc. A* go to:
http://rsta.royalsocietypublishing.org/subscriptions

PHILOSOPHICAL TRANSACTIONS OF THE ROYAL SOCIETY A

Phil. Trans. R. Soc. A (2009) **367**, 3809–3823
doi:10.1098/rsta.2009.0062

Future trends in aberration-corrected electron microscopy

By Harald H. Rose*

Technical University Darmstadt, Institute of Applied Physics, Hochschulstrasse 6, 64289 Darmstadt, Germany

The attainable specimen resolution is determined by the instrumental resolution limit d_i and by radiation damage. Solid objects such as metals are primarily damaged by atom displacement resulting from knock-on collisions of the incident electrons with the atomic nuclei. The instrumental resolution improves appreciably by means of aberration correction. To achieve atomic resolution at voltages below approximately 100 kV and a large number of equally resolved image points, we propose an achromatic electron–optical aplanat, which is free of chromatic aberration, spherical aberration and total off-axial coma. Its anisotropic component is eliminated either by a dual objective lens consisting of two separate windings with opposite directions of their currents or by skew octopoles employed in the TEAM corrector. We obtain optimum imaging conditions by operating the aberration-corrected electron microscope at voltages below the knock-on threshold for atom displacement and by shifting the phase of the non-scattered wave by $\pi/2$ or that of the scattered wave by $-\pi/2$. In this negative contrast mode, the phase contrast and the scattering contrast add up with the same sign. The realization of a low-voltage aberration-corrected phase transmission electron microscope for the visualization of radiation-sensitive objects is the aim of the proposed SALVE (Sub-Å Low-Voltage Electron microscope) project. This microscope will employ a coma-free objective lens, an obstruction-free phase plate and a novel corrector compensating for the spherical and chromatic aberrations.

Keywords: aberration correction; achromatic aplanat; coma-free lens; phase shifter

1. Introduction

The ultimate goal of electron microscopy is to elucidate the three-dimensional atomic structure, the local elemental composition and electronic properties of arbitrary objects. In order to obtain maximum information, we must classify the objects with respect to their inherent structural properties. The extreme cases of total order and total disorder are perfect crystals and entirely amorphous objects. These cases are never realized because ideal crystals hardly exist and the finite size of the atoms gives rise to a certain short-range order in every solid amorphous object. In most cases, it suffices to differentiate between crystalline objects and quasi-amorphous objects. The former objects are extensively investigated in materials science. Owing to the channelling of the electrons along atom columns,

*harald.rose@physik.tu-darmstadt.de

One contribution of 14 to a Discussion Meeting Issue 'New possibilities with aberration-corrected electron microscopy'.

This journal is © 2009 The Royal Society

subsequent elastic scattering processes at the constituent atoms of each column do not appreciably reduce the specimen resolution. Therefore, it is possible to employ relatively thick crystalline objects. Accordingly, we can conceive dynamic electron diffraction in these objects as a tolerable special case of plural electron scattering.

Biological objects and many ceramic materials are important examples of quasi-amorphous objects. To image these objects with high resolution, it is mandatory that they are so thin that plural elastic scattering is negligibly small. This holds true as long as the object thickness is smaller than about one-half of the elastic mean free path length $\Lambda_{\rm e}=1/n_{\rm a}\sigma_{\rm e}$. Here $n_{\rm a}$ and $\sigma_{\rm e}$ are the atom density and the total scattering cross section, respectively, for single-elastic scattering. Most inelastic scattering events are largely delocalized, and the scattering is largely forward directed. Therefore, most subsequent inelastic scattering events do not appreciably change the direction of the elastically scattered electron. As a result, the image formed by the doubly scattered (elastic and inelastic) electrons will provide an image in a chromatic corrected transmission electron microscope (TEM) with about the same resolution as the image formed by the solely elastically scattered electrons. On the other hand, any subsequent elastic scattering event lowers resolution and contrast proportional to the axial distance between the two elastic scattering events.

Radiation damage is the fundamental limitation for the attainable specimen resolution. Solid objects, such as metals, are primarily damaged by atom displacement resulting from knock-on collisions of the electrons with the atomic nuclei. Damage resulting from ionization and/or electronic excitations is generally negligibly small for these objects. Because the closely packed atoms in solid materials form electronic band structures, an ejected electron is immediately replaced by another electron.

The situation differs for biological material. The specimen resolution of these objects is limited by the maximum tolerable dose because the inelastic scattering events destroy chemical bonds by ionization. The missing electron may be replaced within a sufficiently short time by another valence electron, as is the case for the π-electrons of aromatic molecules and of carbon nanotubes. If the binding electron is not replaced within a period of approximately 10 fs, the bond will very likely break and destroy the structure because the strong electric forces rearrange the positions of the atoms (Scherzer 1970). This damage is especially strong for aliphatic molecules because their binding electrons do not form a band structure, as is the case for the π-electrons of aromatic molecules and carbon nanotubes. The electric forces of ionized molecules are generally very strong and rearrange the position of the atoms even if the molecules are embedded in ice or other embedding media. The maximum tolerable dose depends on several processes induced by the interaction of the incident electrons with the sample. The most important processes are atom displacement, surface etching, bond breaking by ionization, heating and chemical etching owing to residual molecules (water). The impact of each of these processes on the tolerable dose is different.

2. Atom displacement

The optimum microscope depends on the object and the kind of information to be obtained. We aim to design the microscope and to elucidate the imaging modes that provide maximum information about the structure of the object for

a tolerable electron dose. Radiation damage resulting from ionization and/or electronic excitations is negligibly small in solid materials such as metals. Owing to the electronic band structure, an ejected electron is immediately replaced by another one. The structure of these objects is primarily damaged by atom displacements resulting from knock-on collisions of the electrons with the atomic nuclei. In order to displace the atom from its position of rest, the transferred energy

$$E_{\mathrm{t}} = E_{\mathrm{tm}} \sin^2 \frac{\theta}{2} \tag{2.1}$$

must be larger than the displacement energy E_{d} of the atom. This energy depends strongly on the direction of the impact and on the position of the atom within the object because the neighbour atoms will take some fraction of the transferred energy. Moreover, the displacement energy for surface atoms is always smaller than that for the bulk atoms. The maximum transferred energy for an elastic head-on collision of an electron with an atom is

$$E_{\mathrm{tm}} \approx \frac{2(1+\gamma)eUm}{M}. \tag{2.2}$$

Here U, m, M and γ denote the accelerating voltage, the rest mass of the electron, the mass of the atom and the relativistic factor, respectively. For carbon and non-relativistic electrons ($\gamma \approx 1$), we obtain $E_{\mathrm{tm}} \approx 1.7 \times 10^{-4}\, eU$. The surface binding energy of carbonaceous material, such as graphite or carbon nanotubes, is of the order of 10 eV. Accordingly, the object will not be damaged if the accelerating voltage is lower than approximately 60 kV.

In order to displace an atom, E_{max} must be larger than the displacement energy E_{d}, or the incident energy of the electron E_0 must exceed the threshold energy E_{th}. Figure 1 demonstrates that the threshold value for surface etching is well below 100 kV for most materials consisting of light atoms. This behaviour supports our conjecture that the bonding energy of atoms located at surfaces or interfaces is much lower than that of the bulk. Thus, displacement (etching) of surface atoms will occur already at rather low voltages. For example, this effect renders extremely difficult the imaging of interfaces and low-dimensional structures, such as nanowalls, nanotubes and nanoparticles.

If the transferred energy is larger than the displacement energy, we find the probability for the displacement of an atom as

$$p_{\mathrm{d}} = D\sigma_{\mathrm{d}}. \tag{2.3}$$

Here D is the maximum tolerable electron dose (number of incident electrons per unit area). The displacement or knock-on cross section is related to the differential elastic scattering cross section via

$$\sigma_{\mathrm{d}} = 2\pi \int_{\theta_{\mathrm{d}}}^{\pi} \sin\theta \frac{\mathrm{d}\sigma_{\mathrm{e}}}{\mathrm{d}\Omega}\, \mathrm{d}\theta. \tag{2.4}$$

We obtain the critical scattering angle θ_{d} for atom displacement by putting $E_{\mathrm{t}} = E_{\mathrm{d}}$ in equation (2.1). All elastic collisions with scattering angles larger than θ_{d} displace the atom. To roughly determine the displacement cross section, it suffices to approximate the atomic potential by the Yukawa potential $\varphi = Z\mathrm{e}^{-r/a}/(4\pi\varepsilon_0 r)$ with screening radius $a \approx 0.05Z^{-1/3}$ nm, where Z denotes the atomic number. For

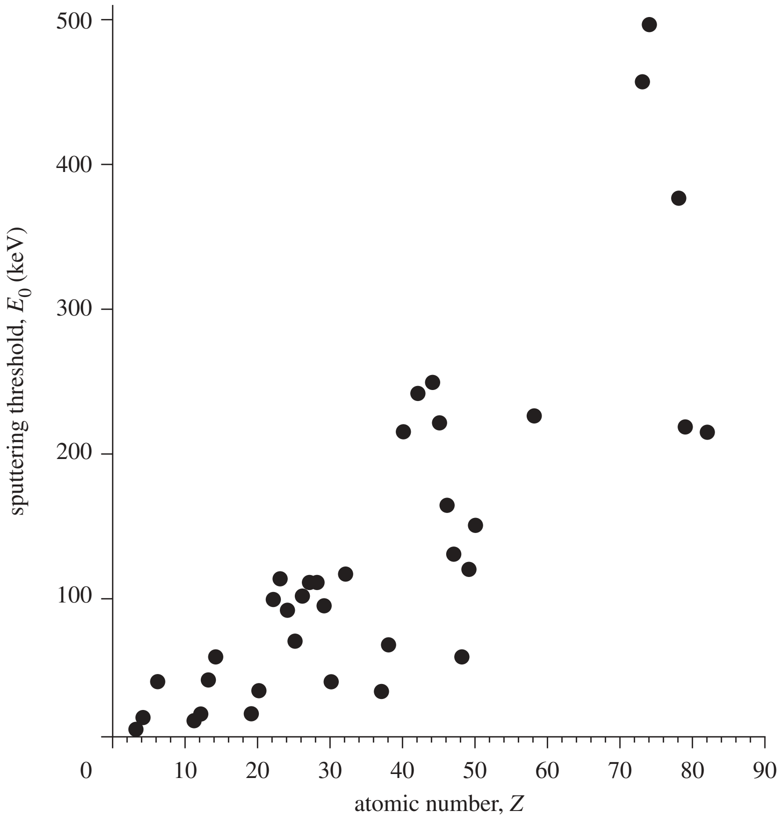

Figure 1. Dependence of sputtering threshold on the atomic number (Hobbs 1987).

this potential, the elastic differential scattering cross section has the form

$$\frac{\mathrm{d}\sigma_\mathrm{e}}{\mathrm{d}\Omega} = f_\mathrm{e}^2(\theta) = \frac{\sigma_\mathrm{et}}{4\pi} \frac{1 + 4k^2 a^2}{[1 + 4k^2 a^2 \sin^2 \theta/2]^2}. \tag{2.5}$$

Here $f_\mathrm{e}(\theta)$ and σ_et are the elastic scattering amplitude of an atom and the total elastic scattering cross section, respectively; $k = 2\pi/\lambda$ is the wavenumber where λ denotes the wavelength. The representation (2.5) of the differential scattering cross section enables an analytical integration of the integral (2.4), giving

$$\sigma_\mathrm{d} = \frac{E_\mathrm{tm} - E_\mathrm{d}}{E_\mathrm{tm} + 4k^2 a^2 E_\mathrm{d}} \sigma_\mathrm{et}. \tag{2.6}$$

The displacement cross section is zero for $E_\mathrm{tm} \leq E_\mathrm{d}$ and approaches the total elastic scattering cross section

$$\sigma_\mathrm{et} \approx \frac{3\pi \alpha^2 Z^2 a^2}{\beta^2} \tag{2.7}$$

at the limit $E_{\mathrm{tm}} \gg 4k^2a^2E_{\mathrm{d}}$; $\alpha \approx 1/137$ is the Sommerfeld constant and

$$\beta = \frac{v}{c} = \frac{\sqrt{2eU^*/E_0}}{1 + eU/E_0}. \tag{2.8}$$

For convenience, we have introduced the relativistic modified acceleration voltage $U^* = U(1 + 2eU/E_0)$, where $E_0 = mc^2 \approx 0.51\,\mathrm{MeV}$ is the rest energy of the electron.

Apart from the total elastic scattering cross section, we need to calculate the effective elastic scattering cross section accounting for the elastically scattered electrons, which pass through the hole of the limiting aperture. Employing the expression (2.5), we obtain

$$\sigma_{\mathrm{e}}(\theta_0) = \sigma_{\mathrm{et}}(1 + 4k^2a^2)\int_0^{\theta_0} \frac{\sin(\theta/2)\cos(\theta/2)}{[1 + 4k^2a^2\sin^2\theta/2]^2}\mathrm{d}\theta = \sigma_{\mathrm{et}}\frac{(1 + 4k^2a^2)\sin^2(\theta_0/2)}{1 + 4k^2a^2\sin^2(\theta_0/2)}. \tag{2.9}$$

As $ka \gg 1$ for voltages larger than approximately 10 kV, we readily derive from the last relation that for $\sin\theta_0/2 \equiv \theta_0/2 > 1/ka$ almost all scattered electrons pass through the hole of the aperture diaphragm.

3. Resolution and contrast

We obtain useful physical insight into the formation of bright-field contrast C by decomposing it into three components, which we define as phase contrast C_{p}, amplitude contrast C_{a} and scattering contrast C_{s}. For this purpose, we subdivide the elastically scattered wave $\psi_{\mathrm{s}} = \psi_{\mathrm{sF}} + \psi_{\mathrm{saF}}$ into the Friedel component ψ_{sF} and the anti-Friedel component ψ_{saF} (Rose 1977). The Friedel component is formed by the Friedel term f_{F} of the complex elastic scattering amplitude $f = f_{\mathrm{F}} + if_{\mathrm{aF}}$, whereas the anti-Friedel part is produced by the anti-Friedel term f_{aF}. This term vanishes in the first-order Born approximation or kinematic approximation, respectively. The Friedel term and the anti-Friedel term are generally complex functions. They are real for a single atom. In this special case, the Friedel term f_{F} coincides with the real part $f_{\mathrm{r}}(\theta)$ and the anti-Friedel term with the imaginary part $f_{\mathrm{i}}(\theta)$ of the elastic scattering amplitude $f(\theta) = f_{\mathrm{r}}(\theta) + if_{\mathrm{i}}(\theta)$. Owing to the chosen decomposition of the scattering amplitude, the phase contrast is given by the interference of the Friedel component ψ_{sF} of the scattered wave with the incident wave ψ_0 at the image plane. Accordingly, the amplitude contrast is formed by the interference of the anti-Friedel term ψ_{saF} of the scattered wave with ψ_0. The scattering contrast $C_{\mathrm{s}} \sim -\psi_{\mathrm{s}}\psi_{\mathrm{s}}^* = -|\psi_{\mathrm{s}}|^2$ is proportional to the negative square of the absolute value of the scattered wave at the image plane. Therefore, this term is always negative whereas the term C_{p} can be positive or negative depending on the phase shift of the scattered wave with respect to the phase of the non-scattered wave. The chosen definition of the phase contrast is reasonable because its integral taken over the entire image plane is zero.

The achievable specimen resolution limit d_{s} of radiation-sensitive objects is predominantly determined by the tolerable dose D of the incident electrons, the image contrast C of an object detail and the signal-to-noise ratio (S/N).

By assuming that the noise and the signal are statistically independent, we eventually obtain

$$d_{\mathrm{s}} = \sqrt{d_{\mathrm{i}}^2 + \frac{(S/N)^2}{C^2 D}}. \tag{3.1}$$

The requirements imposed on the microscope differ for solid specimens and biological objects. Most objects investigated in materials science, such as metals, can tolerate large electron doses D, provided that the electron energy stays below the threshold for atom displacement. In the case $D \to \infty$, the specimen resolution limit approaches the instrumental resolution limit $d_{\mathrm{i}} = 0.61\lambda/\sin\theta_0$ of the electron microscope. However, for most radiation-sensitive objects, the second term of the radicand dominates. This term depends on the maximum tolerable dose D of the incident electrons, the image contrast C and the signal-to-noise ratio S/N, which is necessary to discriminate in the image an object detail from the noise. The minimum value for S/N is approximately 4–5. The tolerable dose is a fixed object-specific quantity. Therefore, we can only decrease the specimen resolution limit by increasing the contrast.

The contrast increases with decreasing instrumental resolution limit and approaches its maximum for $d_{\mathrm{i}} \approx a$. Hence, in order to achieve the highest contrast, the information limit must be smaller than the radius of an atom. In addition, we need a spherically and chromatically corrected objective lens and a phase plate, which shifts the phase of the non-scattered wave by $\pi/2$ or that of the scattered wave by $-\pi/2$. In this case, the phase contrast and the scattering contrast add up with the same sign. Moreover, the acceleration voltage should be kept as small as possible. However, a reduction in the accelerating voltage shortens simultaneously the depth of view

$$t_{\mathrm{v}} \approx d_{\mathrm{s}}^2/\lambda. \tag{3.2}$$

For non-crystalline objects, this depth of view should be somewhat larger than the thickness of the specimen. In order to avoid a loss in specimen resolution, the thickness t of amorphous objects must be smaller than about half the elastic mean free path length $l_{\mathrm{e}} = 1/n\sigma_{\mathrm{e}}$ and thinner than the depth of view (equation (3.1)):

$$\frac{d_{\mathrm{s}}^2}{\lambda} \geq t \leq \frac{1}{2n\sigma_{\mathrm{e}}}. \tag{3.3}$$

The atom number density n is approximately $0.1\,\text{Å}^{-3}$ for most amorphous biological materials.

We obtain maximum phase contrast in the ideal case of an aberration-free objective lens and a phase plate, which shifts the phase of the scattered wave by $\pm\pi/2$ in the case of weak phase objects. The maximum achievable phase contrast in the image of a single atom in the first-order Born approximation is

$$\begin{aligned} C_{\mathrm{p}}(\theta_0) &= \pm\frac{4\pi}{\lambda}\int_0^{\theta_0} f_{\mathrm{B}}(\theta)\sin\theta\,\mathrm{d}\theta \\ &= \pm 2\sqrt{3}\frac{\alpha Z}{\beta}\ln\left(1 + 4k^2 a^2 \sin^2\left(\frac{\theta_0}{2}\right)\right) \approx \pm\frac{Z}{37\beta}\ln\left(1 + \frac{14a^2}{d_{\mathrm{i}}^2}\right). \end{aligned} \tag{3.4}$$

By employing the optical theorem (Rose 1984), the amplitude contrast is roughly given by the equation

$$C_{\mathrm{a}} \approx -\frac{\sigma_{\mathrm{e}}(\theta_0)}{a^2+d_{\mathrm{i}}^2} \approx -\frac{3\pi}{\beta^2}\frac{\alpha^2 Z^2}{1+d_{\mathrm{i}}^2/a^2}\frac{(1+4k^2a^2)\sin^2(\theta_0/2)}{1+4k^2a^2\sin^2(\theta_0/2)}. \tag{3.5}$$

We find the dependence of the relative velocity $\beta = v/c$ on the voltage U from expression (2.8) and that of the wavelength from the relation

$$d_{\mathrm{i}} = \frac{0.61\lambda}{\sin\theta_0} = \frac{0.75}{\sin\theta_0}\sqrt{\frac{\mathrm{Volt}}{U^*}}\ \mathrm{nm}. \tag{3.6}$$

To survey the dependence of the amplitude contrast on the instrumental resolution, we assume $ka \gg 1$. Considering the relations (2.8) and (3.5), we obtain

$$C_{\mathrm{a}} \approx -\frac{42\pi}{\beta^2}\frac{\alpha^2 Z^2 a^4}{d_{\mathrm{i}}^4}\frac{1}{1+14a^2/d_{\mathrm{i}}^2}. \tag{3.7}$$

The formula shows that for a fixed instrumental resolution limit the amplitude contrast is inversely proportional to the square of the electron velocity, whereas the phase contrast (equation (3.3)) is inversely proportional to β. Hence, the amplitude contrast increases much stronger with decreasing voltage than the phase contrast. The ratio

$$\frac{C_{\mathrm{p}}}{C_{\mathrm{a}}} \approx \pm 3.6\frac{\beta}{Z}\frac{d_{\mathrm{i}}^4}{a^4}\left(1+\frac{14a^2}{d_{\mathrm{i}}^2}\right)\ln\left(1+\frac{14a^2}{d_{\mathrm{i}}^2}\right) \tag{3.8}$$

demonstrates that for $d_{\mathrm{i}} \geq 3a$, the phase contrast of a single atom exceeds the amplitude contrast by far. Our results do not hold true if several atoms are located in the shadow of each other as is the case for crystalline objects whose atom columns are aligned parallel to the direction of the incident electrons.

So far, we have disregarded the inelastic scattered electrons by supposing that they are removed from the image formation by an imaging energy filter. The use of these electrons will greatly enhance S/N if the object is appreciably thicker than the inelastic mean free path length, as usually happens for biological objects embedded in ice. In this case, many electrons are scattered more than once. These electrons may undergo two or more inelastic scattering events or one inelastic and one elastic scattering process. The inelastic scattering lowers the elastic scattering amplitude. Hence, the phase contrast is reduced. Fortunately, if an inelastic scattered electron undergoes an additional elastic scattering process, the scattered part of the wave is coherent with its non-scattered part. Unfortunately, the resulting image will be blurred by chromatic aberration. Hence, to enhance contrast and specimen resolution, we must compensate for both chromatic and spherical aberration.

4. Bright-field image of a single atom

In order to survey the formation of contrast in the case of high-resolution bright-field imaging, we discuss the intensity in the image of a single atom obtained by an ideal objective lens and a phase plate shifting the phase

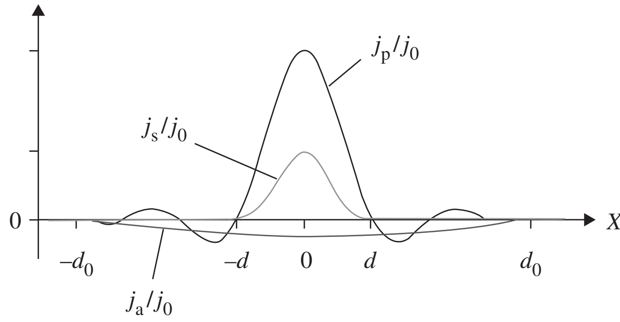

Figure 2. Parts of the normalized current density distribution forming the bright-field image of an atom in an aberration-corrected TEM equipped with an ideal phase plate.

of the elastically scattered wave by $\pm\pi/2$ for scattering angles larger than θ_p up to the limiting angle θ_0 defined by the radius of the opening of the aperture. For convenience, we refer the current density to the object plane. The current density is a function of the radial distance ρ from the centre of the atom:

$$j(\rho) = j_0 + j_p(\rho) + j_a(\rho) + j_s(\rho). \tag{4.1}$$

The first term on the right-hand side describes the constant background current density j_0. The second term is the current density

$$j_p \approx \pm j_0 \frac{|f(0)|}{\rho}\{\theta_0 J_1(k\theta_0\rho) - \theta_p J_1(k\theta_p\rho)\} \tag{4.2}$$

produced by the ideal phase plate shifting the phase of the scattered wave by $\pm\pi/2$ in the angular range $\theta_p \leq \theta \leq \theta_0$. The function $J_1(x)$ is the first-order Bessel function. The contribution

$$j_a \approx -2j_0\pi\theta_p^2 \frac{\sigma_t}{\lambda^2} \frac{J_1(k\theta_p\rho)}{k\theta_p\rho} \tag{4.3}$$

results from the interference of the anti-Friedel component of the scattered wave with the non-scattered electron wave. The value $j_a(0)/j_0 = -C_a \approx -\pi\theta_p^2\sigma_t/\lambda^2$ determines the amplitude contrast C_a. This contrast becomes negligibly small in the limit $\theta_p \to 0$ as demonstrated schematically in figure 2.

The last term

$$j_s \approx j_0\pi\theta_0^2 \frac{\sigma(\theta_0)}{\lambda^2} \left[\frac{2J_1(k\theta_0\rho)}{k\theta_0\rho}\right]^2 \tag{4.4}$$

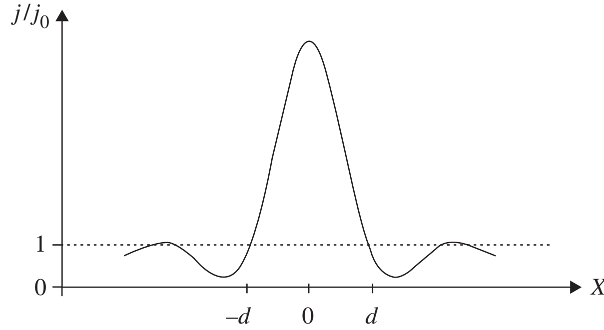

Figure 3. Schematic distribution of the normalized current density in the bright-field image of an atom in the case of optimum negative contrast.

gives rise to the scattering contrast $C_s = -j_s(0)/j_0 \approx -\pi\theta_0^2\sigma(\theta_0)/\lambda^2$. In the absence of the phase plate ($\theta = \theta_0$), the phase contrast current vanishes. The resulting total contrast

$$C_t = C_s + C_a \approx \pi\theta_0^2 \frac{\sigma_t - \sigma_a}{\lambda^2} = \pi\theta_0^2 \frac{\sigma_a}{\lambda^2} \approx \frac{\sigma_a}{d_i^2} \tag{4.5}$$

is the so-called scattering absorption contrast, which is proportional to the cross section

$$\sigma_a = 2\pi \int_{\theta_0}^{\pi} \frac{d\sigma_e(\vartheta)}{d\Omega} \sin\vartheta \, d\vartheta. \tag{4.6}$$

The ratio σ_a/σ_t determines the fraction of the elastically scattered electrons removed by the aperture diaphragm. In the absence of this diaphragm, the total contrast is zero because all electrons originating from a point scatter are redirected by the ideal lens into the conjugate image point yielding uniform image intensity. The amplitude contrast is always positive because it accounts for the intensity carried away by the scattered electrons. The scattered electrons passing through the hole of the aperture diaphragm and hitting the image spot enhance the central intensity. Therefore, they always produce a negative contrast. The phase contrast $C_p = -j_p(0)/j_0$ may be positive or negative depending on the sign of the phase shift. We obtain maximum negative contrast $C = C_a + C_s + C_p$ if we choose the angle θ_p as small as possible and shift the phase of the scattered wave by $-\pi/2$. To visualize structural details with a large range of spatial frequencies we aim for ratios $\theta_0/\theta_p \geq 100$.

The negative contrast mode shown in figure 3 has the advantage that the central current density can adopt arbitrarily large values, at least in principle, resulting in a very high negative contrast.

We obtain positive total contrast shown in figure 4 by shifting the phase of the scattered wave by $\pi/2$, as approximately realized for a small range of spatial frequencies in the standard TEM operating under Scherzer conditions (Scherzer 1949). By comparing figures 3 and 4, we readily conceive the advantage of operating the microscope in negative contrast mode. The experimental results of Urban (2008) and co-workers impressively demonstrate our findings, which we have derived from a simple single-atom model.

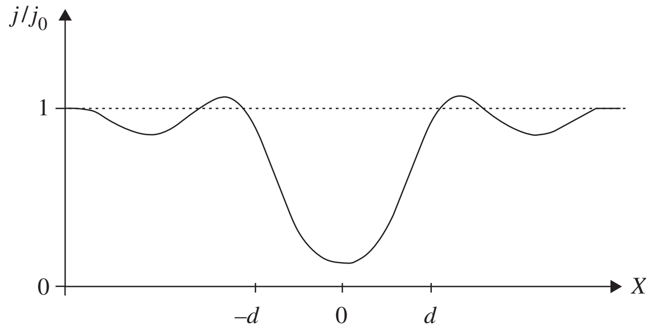

Figure 4. Schematic distribution of the normalized current density in the bright-field image of an atom in the case of maximum positive contrast.

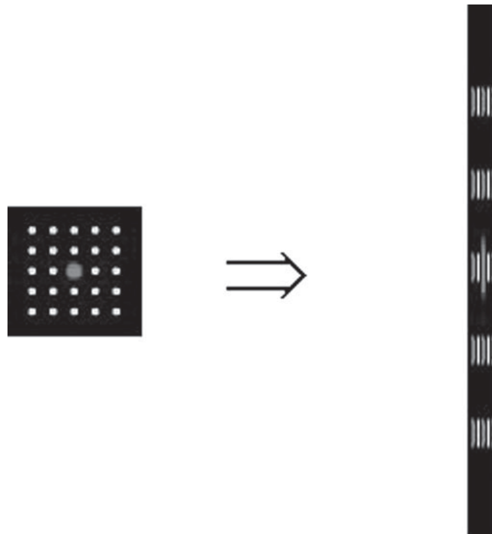

Figure 5. Formation of an anamorphotic image of the diffraction plane.

5. Design of an obstruction-free phase plate

The incorporation of an adjustable electrostatic potential is a very promising method to realize Zernike-type phase contrast. In order to avoid obstruction by the field-forming electrodes, it is advantageous to perform the phase shift at a strongly anamorphotic image of the diffraction plane (Schroeder *et al.* 2007). Such a strongly first-order distorted stigmatic image can only be obtained by an appropriate quadrupole system, which enlarges the diffraction pattern in one direction and compresses it in the orthogonal direction, as illustrated schematically in figure 5.

The line-shaped image enables us to shift the phase of the scattered wave without any obstruction by means of the micro-phase plate depicted in figure 6. We can consider this phase plate as the superposition of a quadrupole with a cylinder lens, such that the potential has a saddle point at the centre of

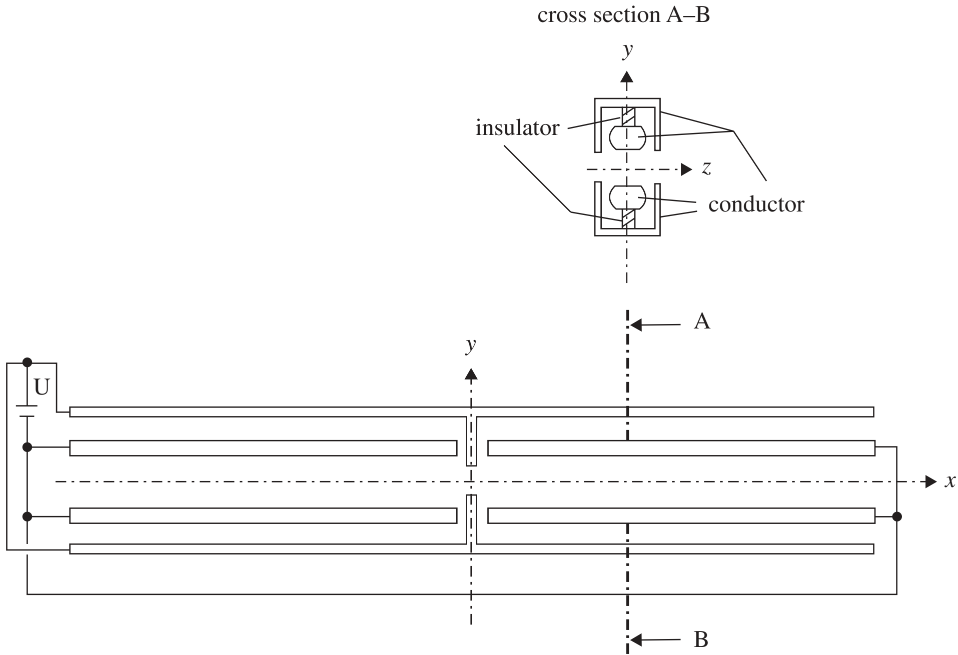

Figure 6. Scheme of the obstruction-free phase plate placed at strongly anamorphotic images of the diffraction plane.

the anamorphotic image of the diffraction plane. In order to obtain a large range of constant phase shift, we aim for an aspect ratio of the anamorphotic image that is larger than 100. First investigations have shown that such aspect ratios are achievable in practice by means of a novel system, which represents in combination with the phase plate an obstruction-free *phase shifter*. We obtain optimum phase shift by incorporating two phase plates, each of which is positioned at one of the two orthogonal anamorphotic images of the diffraction plane. Each phase plate shift introduces a phase shift of $\pi/4$ between the scattered wave and the non-scattered wave.

6. Achromatic aplanats

The new generation of CCD cameras enables the recording of large image fields. For example, the transfer of a large field of view is necessary if we want to image a large number of identical species such as ribosomes. The reduction of the instrumental resolution limit $d_{\mathrm{i}} \approx 0.61\lambda/\theta_0$ by the correction of the spherical aberration is accompanied by an increase in the usable aperture angle θ_0. The resolution limit stays constant if we enlarge the wavelength in proportion to θ_0. Hence, atomic resolution at low voltages requires large aperture angles. However, the deleterious influence of the electrical and mechanical instabilities on the attainable information limit strongly increases by enlarging the aperture. Therefore, usable aperture angles larger than approximately 50 mrad can hardly be achieved with the present technology.

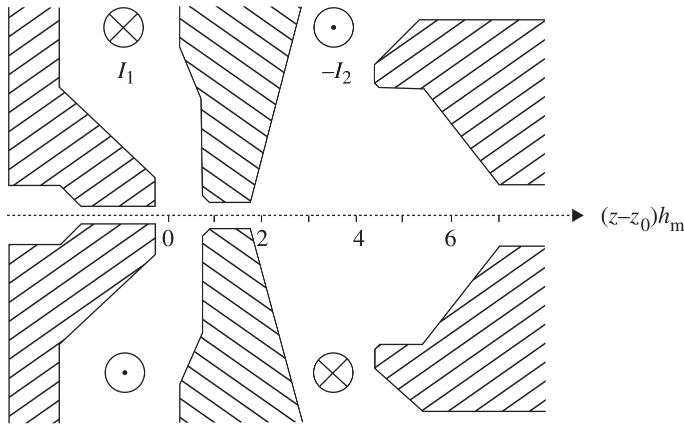

Figure 7. Schematic arrangement of the pole pieces of the coma-free magnetic lens. The characteristic reciprocal length $h_m = B_{max}(e/8m_e\Phi^*)^{1/2}$ is determined by the maximum magnetic flux density B_{max} and the relativistic modified accelerating voltage Φ^*.

The attainable number N of equally resolved object points per diameter of the image field

$$N \approx \frac{1}{3|K|\theta_0^2} \tag{6.1}$$

is determined by the complex coefficient $K = K_r + iK_i$ of the off-axial coma and the aperture angle. We can eliminate the coefficient K_r of the isotropic coma by matching the coma-free point of the objective lens with that of the corrector. Unfortunately, this is not possible for the coefficient K_i of the anisotropic or azimuthal coma introduced by the aperture dependence of the Larmor rotation within magnetic lenses. This value is approximately 0.5 for most objective lenses employed in high-resolution electron microscopes. Using this value and the maximum aperture angle $\theta_0 = 50$ mrad, relation (6.1) gives $N \approx 290$. In order to achieve 2000 equal image points per image diameter at these operation conditions, we must also compensate for the anisotropic coma of the objective lens.

A lens system forms a so-called aplanat if it is free of spherical aberration and off-axial coma. For these systems, the number of image points is limited by field curvature and field astigmatism. These aberrations depend on the square of the lateral distance of the object points. To obtain atomic resolution at low voltages and a large field of view, we must employ an achromatic aplanat. As sextupoles cannot compensate for chromatic aberrations, we must use electric and magnetic quadrupoles for the chromatic correction and octopoles for eliminating the spherical aberration. For voltages below approximately 100 kV, we can use the coma-free magnetic objective lens depicted schematically in figure 7. This compound lens does not introduce anisotropic coma. It consists of a strong short lens at the object plane z_o, followed by a somewhat weaker extended lens whose field tapers off in a nearly linear tail. The directions of the currents within the two lenses are opposite. If we tolerate anisotropic coma, the lens can also be used as a Lorentz lens with a short focal length. By reducing the current of the first winding and enhancing it in the second coil, we can nullify the magnetic field

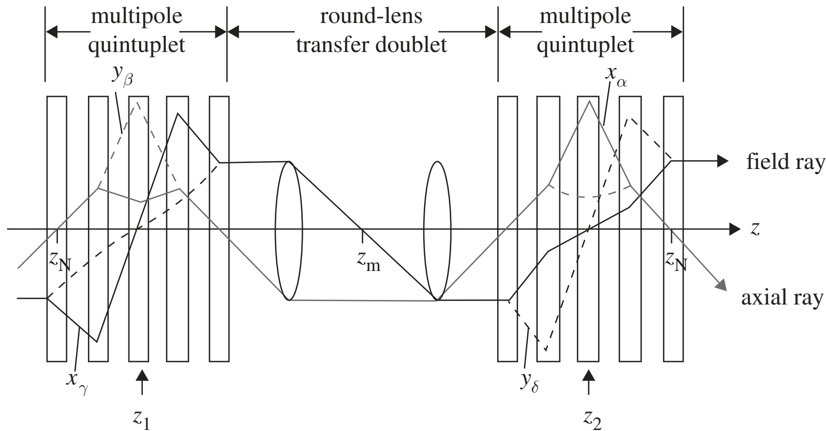

Figure 8. Schematic setup of the TEAM corrector; anamorphotic images of the diffraction plane are formed at the centres z_1 and z_2 of each telescopic multipole quintuplet producing quadrupole and octopole fields.

at the object plane without unduly enlarging the focal length of the lens, which adopts the properties of a probe-forming lens. Hence, the coma-free lens is well suited for *in situ* applications.

The highest attainable specimen resolution is a function of the tolerable dose, the object thickness, the threshold electron energy for atom displacement, the contrast and the required signal-to-noise ratio. To maximize this ratio, we must use as many scattered electrons as possible. We can largely meet this condition by incorporating an achromatic aplanat and an obstruction-free phase shifter into a TEM whose accelerating voltage can be varied according to the requirements imposed by the object. In order to increase S/N and contrast, the instrumental resolution limit must be made as large as possible. At present, the parasitic electrical and mechanical instabilities pose the main obstacle because they prevent an appreciable reduction of the information limit rather than the residual defects of the aberration-corrected lens system. The incorporation of the achromatic aplanat into the electron microscope enables large illumination angles because all directions of incidence represent coma-free axes. Moreover, the correction of chromatic and spherical aberration allows sufficient space for the sample necessary for *in situ* applications. The TEAM corrector shown schematically in figure 8 is the proper *achroplanator*. It consists of a telescopic round-lens transfer doublet and two telescopic multipole quintuplets. An appropriate corrector must include crossed electric and magnetic quadrupoles, compensating for the chromatic aberration and octopoles eliminating the spherical aberration. The TEAM corrector uses the symmetry principles of the hexapole corrector (Rose 1990), which can only compensate for the spherical aberration of the objective lens. To enable the correction of chromatic and spherical aberrations, each of the two hexapole elements is replaced by a symmetric telescopic multipole quintuplet. Within these elements, electric and magnetic quadrupole fields are excited, which produce an appropriate astigmatic path of rays and compensate for the chromatic aberration of the round lenses. Additional octopole fields eliminate the

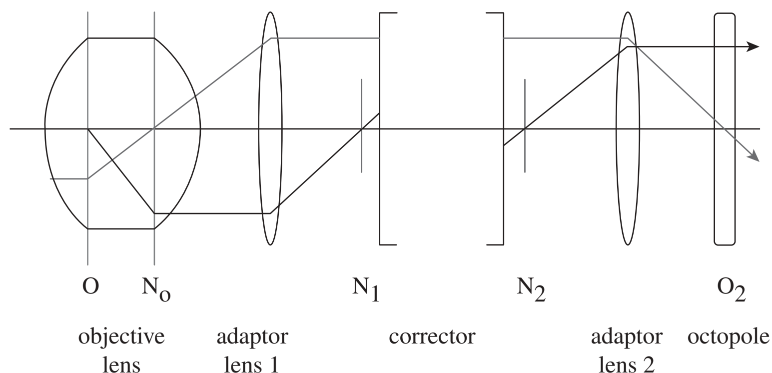

Figure 9. Arrangement of the elements of the achromatic aplanat and course of the fundamental axial ray and field ray.

spherical aberration without introducing off-axial coma. The achroplanator yields in combination with the coma-free objective lens an achromatic electron aplanat for voltages in the range of approximately 20–100 kV, as depicted schematically in figure 9. The realization of such a microscope is the aim of the SALVE (Sub-Å Low-Voltage Electron microscope) project proposed by Ute Kaiser.

7. Conclusion

The development of the electron microscope has made unprecedented progress owing to the successful realization of aberration correctors (Haider *et al.* 1998), monochromators and high-performance energy filters (Rose 2005). The optimum operation mode of aberration-corrected electron microscopes depends strongly on the material of the object and on the properties to be investigated. To avoid atom displacement, the accelerating voltage must be lower than the knock-on threshold. In order to achieve sub-Å resolution at low acceleration voltages, we must correct the chromatic and the spherical aberration of the imaging system and reduce the information limit below 1 Å. This mandatory reduction poses very demanding requirements on the electric and mechanical stabilities. Electron spectroscopic imaging with an energy resolution below 0.2 eV requires the incorporation of a monochromator and a high-performance imaging energy filter into the electron microscope. The resolution of the image of an infinitely radiation-resistant specimen is solely determined by the instrumental resolution. In this ideal case, it is advantageous to increase the acceleration voltage in order to investigate relatively thick objects. However, real samples are always influenced (damaged) by the electron beam and thus the tolerable duration for observing the sample in the undamaged state becomes an issue.

Two classes of materials will benefit from using low voltages for image formation. (i) Conducting solid materials, such as metals and nanotubes, will not be damaged at voltages below the threshold for surface etching. Moreover, the objects will be imaged with very high contrast at these voltages. (ii) For insulators and organic materials, two properties are in concurrence when going to lower voltages: the increase in radiation damage for fixed dose and the increase

in contrast. It has been experimentally shown that with decreasing voltage, contrast increases faster than damage (Hayashida *et al.* 2006) because we need an appreciably lower dose for obtaining the same S/N.

8. Summary

In the last decade, unprecedented progress has been made in the development of the electron microscope, which has advanced from an instrument producing merely pictures to an analytical instrument yielding quantitative information about the structure, the chemical composition and the electronic properties of objects on an atomic scale. To fully exploit the capabilities of the electron microscope, it is necessary to compensate for the primary chromatic aberration, spherical aberration and the off-axial coma by means of an appropriate achroplanator. The introduction of a monochromator and a high-performance in-column energy filter such as MANDOLINE will enable local spectroscopy with an energy resolution below 0.1 eV. Finally, the application of low voltages and the development of an obstruction-free phase shifter will appreciably improve the specimen resolution in images of radiation-sensitive objects such as nanotubes, ceramics and molecules to name only a few.

I want to thank Professor U. Kaiser (Ulm) for valuable discussions and Professor R. Schroeder (Heidelberg) for putting figure 5 at my disposal.

References

Haider, M., Rose, H., Uhlemann, S., Schwan, E., Kabius, B. & Urban, K. 1998 A spherical-aberration-corrected 200 kV transmission electron microscope. *Ultramicroscopy* **75**, 53–60. (doi:10.1016/S0304-3991(98)00048-5)

Hayashida, M. T., Kawasaki, T., Kimura, T. Y. & Takai, Y. 2006 Estimation of suitable condition for observing copper–phthalocyanine crystalline film by transmission electron microscopy. *Nucl. Instrum. Methods Phys. Res. B* **248**, 273–278. (doi:10.1016/j.nimb.2006.04.168)

Hobbs, L. W. 1987 Radiation effects in analysis by TEM. In *Introduction to analytical electron microscopy* (eds J. J. Hren, J. I. Goldstein & D. C. Joy), pp. 399–445. New York, NY: Plenum Press.

Rose, H. 1977 Nonstandard imaging methods in electron microscopy. *Ultramicroscopy* **2**, 251–267. (doi:10.1016/S0304-3991(76)91538-2)

Rose, H. 1984 Information transfer in transmission electron microscopy. *Ultramicroscopy* **15**, 173–192. (doi:10.1016/0304-3991(84)90038-X)

Rose, H. 1990 Outline of a spherically corrected semi-aplanatic medium-voltage TEM. *Optik* **85**, 19–24.

Rose, H. 2005 Prospects for aberration-free electron microscopy. *Ultramicroscopy* **103**, 1–6. (doi:10.1016/j.ultramic.2004.11.017)

Scherzer, O. 1949 The theoretical resolution limit of the electron microscope. *J. Appl. Phys.* **20**, 20–29. (doi:10.1063/1.1698233)

Scherzer, O. 1970 Die Strahlenschädigung der Objekte als Grenze der hochauflösenden Elektronenmikroskopie. *Ber. Bunsen-Ges. Phys. Chem.* **74**, 1154–1167.

Schroeder, R., Barton, B., Rose, H. & Benner, G. 2007 Contrast enhancement by anamorphotic phase plates in an aberration-corrected TEM. *Microsc. Microanal.* **13**(Suppl. 3), 8–9. (doi:10.1017/S143192760708004X)

Urban, K. 2008 Studying atomic structures by aberration-corrected transmission electron microscopy. *Science* **321**, 505–510. (doi:10.1126/science.1152800)